Title Page

Propagation phase-contrast micro-computed tomography allows laboratory-based three-dimensional imaging of articular cartilage down to the cellular level

Jeffrey N. Clark †*, Amin Garbout ‡, Silvia A. Ferreira ¥, Behzad Javaheri ¶, Andrew A. Pitsillides ¶, Sara M. Rankin ¥, Jonathan R.T. Jeffers †, Ulrich Hansen †

† Department of Mechanical Engineering, Imperial College London, London, UK

‡ Imaging and Analysis Centre, Natural History Museum London, London, UK

¥ National Heart & Lung Institute, Faculty of Medicine, Imperial College London, London, UK

¶ Skeletal Biology Group, Comparative Biomedical Sciences, Royal Veterinary College, UK

Co-author email addresses: j.clark14@imperial.ac.uk; amin.garbout@gmail.com;

s.ferreira@imperial.ac.uk; bjavaheri@rvc.ac.uk; apitsillides@rvc.ac.uk; s.rankin@imperial.ac.uk;

j.jeffers@imperial.ac.uk; u.hansen@imperial.ac.uk

*Corresponding author: j.clark14@imperial.ac.uk, 774 City and Guilds Building, South Kensington Campus, Imperial College, SW7 2AZ, UK

Abstract

(1) Objective

High-resolution non-invasive three-dimensional (3D) imaging of chondrocytes in articular cartilage remains elusive. The aim of this study was to explore whether laboratory micro-computed tomography (micro-CT) permits imaging cells within articular cartilage.

(2) Design

Bovine osteochondral plugs were prepared four ways: in phosphate-buffered saline (PBS) or 70% ethanol (EtOH), both with or without phosphotungstic acid (PTA) staining. Specimens were imaged with micro-CT following two protocols: 1) absorption contrast (AC) imaging 2) propagation phase-contrast (PPC) imaging. All samples were scanned in liquid. The contrast to noise ratio (C/N) of cellular features quantified scan quality and were statistically analysed. Cellular features resolved by micro-CT were validated by standard histology.

(3) Results

The highest quality images were obtained using propagation phase contrast imaging and PTA-staining in 70% EtOH. Cellular features were also visualised when stained in PBS and unstained in EtOH. Under all conditions PPC resulted in greater contrast than AC ($p < 0.0001$ to $p = 0.038$). Simultaneous imaging of cartilage and subchondral bone did not impede image quality. Corresponding features were located in both histology and micro-CT and followed the same distribution with similar density and roundness values.

(4) Conclusions

Three-dimensional visualisation and quantification of the chondrocyte population within articular cartilage can be achieved across a field of view of several millimetres using laboratory-based micro-CT. The ability to map chondrocytes in 3D opens possibilities for research in fields from skeletal development through to medical device design and treatment of cartilage degeneration.

Keywords: osteoarthritis, chondrocyte, imaging, micro-CT, articular cartilage, 3D

Running headline: Imaging chondrocytes in three-dimensions

Introduction

Research into the structure of articular cartilage has been performed for over a century[1] but has historically been limited to destructive 2D imaging on a single plane[2]. There is potential for micro-computed tomography (micro-CT) to reveal full-field 3D information from intact segments of articular cartilage. Success could advance the study of osteoarthritis development and provide a natural pattern to enable full-field strain measurements of cartilage[3]. This could lead to advancements in chondral repair scaffolds that target biomimicry, as is possible with other tissues[4]. Articular cartilage is typically difficult to image by micro-CT due to poor absorption of X-rays owing to its composition of low-Z elements such as carbon, hydrogen, oxygen and nitrogen[5]. However, two methods that exist to increase contrast in cartilage are contrast agents[6] and phase contrast imaging[7].

Contrast agents, typically composed of high-density heavy metals, bind to extracellular components, increasing density and thereby increase the resulting signal[8]. Articular cartilage has been stained for micro-CT to study morphological changes[9, 10], glycosaminoglycan content[11, 12] and to infer the spatial distribution of collagen and assessment of degradation[13]. Pauwels *et al.,* conducted an investigation of 28 potential contrast agents and found that the most promising contrast agents for soft-tissue staining were phosphomolybdic acid ($H_3PMo_{12}O_{40}$, PMA), phosphotungstic acid ($H_3PW_{12}O_{40}$, PTA) and mercury chloride ($HgCl_2$)[6]. PTA and PMA have been used to indicate collagen distribution[14]. Whilst it is proposed that these stains may bind to various proteins[5], the underpinning mechanism(s) is not fully elucidated[15]. Many of these studies have involved the use of ethanol (EtOH) as the solvent to dissolve the contrast agent[14], whilst others fully desiccate the cartilage to enable the structure to be observed[16]. These changes in water content likely modify the mechanical properties of the material and thus may not be fully representative of the *in vivo* conditions. Imaging samples immersed in alternative liquids, altering less the physiological conditions, would be attractive.

Phase contrast imaging detects the phase shift that X-rays experience passing through matter, resulting from differences in refractive index or non-uniform thicknesses[17]. It is particularly useful for low-contrast biological samples in life-sciences[18, 19]. Three of the most common techniques are propagation phase contrast (PPC)[20], analyser-based imaging[21] and grating interferometry[22]. Many of these methods, including both analyser-based diffraction enhanced contrast and grating interferometry, require specialised and modified equipment. PPC requires no such modification to the equipment used for typical absorption contrast as long as the beam is highly spatially coherent and the scanner allows for the detector to be positioned sufficiently far from the sample. Various attempts have been made to image articular cartilage with phase contrast using relatively common laboratory micro-CT[23, 24] as well as highly specialised synchrotron sources[7, 25]. Data indicates PPC in the synchrotron is able to detect the structure of cartilage[26], but lab micro-CT has not yet generated comparable images[25, 27]. The ability to image the cartilage structure in lab micro-CT would be highly advantageous, enabling wider access for researchers in utilising technology which may eventually allow *in vivo* diagnostics with clinically-available tomography.

Herein we explore the hypothesis that a combination of staining and laboratory phase-contrast micro-CT can adequately visualise individual chondrocytes within intact samples of articular cartilage. Our primary aim was to develop a method to image chondrocytes with laboratory micro-CT. Our secondary aim was to achieve this whilst maintaining the tissue in conditions which deviate the least from those found physiologically.

Method

Sample preparation

Fresh juvenile bovine (<2 years old) stifle joints (n = 3) from two animals were obtained from a slaughterhouse and stored at -25 °C until experimentation. The specimens were thawed at 4 °C, kept hydrated with Dulbecco's phosphate buffered saline solution (DPBS, #14190-094, Fisher Scientific, USA) and 3 mm cylindrical osteochondral plugs (n = 10) were taken from the femoral condyles using a hollow punch. Samples were prepared under four conditions (**Fig. 1**). All were initially bathed for 30 minutes in PBS and the ethanol (EtOH) treated samples were immersed in step-wise increasing concentrations of EtOH[28]. From each of the PBS or EtOH treated groups, one osteochondral plug was maintained in the liquid without staining (denoted PBS or EtOH), whilst others (Table 1 and supplementary table) were further processed with staining using a 1% w/v phosphotungstic acid solution (weight/volume, $H_3PW_{12}O_{40}$, PTA, #79690 Sigma-Aldrich, USA) in either PBS or 70% ethanol for 21 hours then rinsed in the medium prior to micro-CT scanning (denoted PBS+PTA or EtOH+PTA). The full description of each sample is included in the supplementary table. Staining time was optimised in pilot experiments. All samples were stored in their liquid medium at room temperature prior to scanning.

[Suggested placement for Figure 1]

X-ray micro-tomography scanning

Samples were immersed in their corresponding liquid medium (PBS or 70% EtOH) and mounted in sealed plastic containers. All scans were carried out on a Versa 520 X-ray micro-CT scanner (Zeiss, Germany). For all scans, voltage and current were 40 kV and 75 µA respectively with no pixel

74 binning. No x-ray filters were applied. To allow comparison of the signal between absorption and
75 propagation phase signals, scans under different scanning protocols were taken. Image quality at
76 different source-to-object (SOD) and object-to-detector (ODD) distances can be maintained by
77 adjusting exposure time to ensure a sufficient photon count reaches the detector. The larger the
78 SOD and ODD distances, the longer the exposure time required to maintain the photon count. Firstly
79 the absorption signal was collected by minimising the SOD and ODD distances to reduce scanning
80 time. This is the type of scan typically carried out with a micro-CT scanner. Next the phase contrast
81 scan was taken with enlarged SOD and ODD, allowing implementation of propagation phase contrast
82 (PPC). Using a larger SOD also has the advantage of decreasing cone beam error[29]. Increasing the
83 ODD for the PPC scan reduced the X-ray flux, resulting in exposure times typically four times longer
84 than for the absorption scan. The full set of scan parameters for each scan are shown in Table 1 and
85 in the supplementary table. A volume of interest of approximately 2x2x2 mm was included for each
86 set of conditions. For the bovine samples used during this study, the volume of interest did not
87 constitute the entire cartilage height. For histological comparison, an additional sample (e) was
88 prepared by the same method employed for the EtOH+PTA sample (d) and scanned to maximise
89 image quality with a higher number of projections and further increased SOD and ODD.
90 Reconstruction of the projection images to produce 3D volumetric data sets was performed using
91 the Reconstructor Scout-and-Scan software (Zeiss, Germany). The reconstructed CT volumes were
92 visualized and analysed using (Fiji Is Just) ImageJ software[30] (version 1.52g, NIH, USA). Two of the
93 sample from groups PBS+PTA (b) and EtOH+PTA (d) were scanned twice using PPC to ensure scan
94 repeatability and measure consistency in scan quality.

95

96 **Histology**

97

Following the micro-CT scan, one of the osteochondral plugs (e) was stored in 10% neutral buffered formalin (#HT501128, Sigma-Aldrich) for 24 hours. Before paraffin wax embedding, PTA was removed by ion-exchanging in a washing solution of 0.55 mM NaOH, 0.1 M of Na_2HPO_4, 137 mM NaCl, and 2.7 mM KCl, pH 10 for 5 days following established protocol[31]. The sample was subsequently decalcified in 425 mM EDTA neutral solution for 7 days exchanged every day[32], paraffin-embedded and sections (5 µm) collected on Superfrost slides (Fisher Scientific, USA). Sections were dewaxed immersing twice for 5 minutes in Gentaclear (Genta Medical, UK), washed in tap water and subsequently stained with: (1) Alcian Blue at pH 2.5 with counterstaining of nuclei with Neutral Red[33]; (2) Masson's Trichrome[32]; (3) Picro-Sirius Red[34] or (4) Safranin O (0.5%)/Fast Green FCF(0.2%) with nuclei counterstained with Celestin blue and Harris Haematoxylin (all from Sigma-Aldrich, USA)[35]. All sections slides were cover slipped with DPX mountant (Sigma-Aldrich, USA). Colour micrographs were acquired using a Zeiss Axio Observer Inverted Widefield Microscope with an IC5 colour camera, and with a fully motorised stage controlled by ZEN Blue pro software capable of tiling and stitching, using a 20× DIC Plan Apochromat air objective with numerical aperture of 0.8, and 2048 × 2048 resolution, with pixel size corresponding to 0.33 µm.

Image analysis

Contrast to Noise Analysis

Of the constituent components within articular cartilage, the largest individual features are chondrocytes. Yet the chondrocytes have previously been difficult to visualise over large distances in 3D[36], owing to their small size, low spatial density and previously discussed low contrast. Typically each chondrocyte will occupy few voxels and noise can easily lead to erroneous segmentation. Therefore, as a measure of contrast and scan quality, the contrast to noise ratio (C/N) of individual

chondrocyte features was calculated through the sample height for each sample and compared between the samples scanned under different conditions. Within each sample (**Fig. 2**.A) a region was micro-CT scanned (**Fig. 2**.B). Eleven equally spaced layers per sample from the reconstructed image stack (**Fig. 2**.C) were analysed in ImageJ using the Plot Profile tool (**Fig. 2**.D & E) with a line length of 60 pixels to measure grayscale intensity across cells and their surrounding matrix (n = 10 per layer, n = 110 cells per sample)[20]. Chondrocytes were visualised with a higher grayscale value than the surrounding matrix. A higher C/N indicates more clearly visualised features. Care was taken to only include one chondrocyte per profile therefore only the highest peak characterised a cell, all others represented the surrounding matrix. A MATLAB script (R2016a, MathWorks Inc, Natick, MA, USA) computed the ratio of the amplitude of the maximum peak (A) above the background peaks for each plot, divided by the standard deviation of the surrounding noise peaks[37] (**Fig. 2**.E).

[Suggested placement for Figure 2]

Histological Analysis

The micro-CT and histological images for sample (e) were manually registered in ImageJ. Similarly located areas of 500 µm x 500 µm were selected in both modalities (micro-CT n = 12, histology n = 3 for each of the four stains) at three different heights through the sample (n = 36 in total each for micro-CT and histology). Three consecutive micro-CT slices were combined using the Max Intensity Z project process within Fiji ImageJ software to result in a comparable thickness (5.91 µm) to that of the histological slices (5 µm). The histological images were scaled to the same resolution as the micro-CT. Images were segmented using the Trainable Weka Segmentation[38] and the Analyze Particles tool was used with a minimum size of 5 μm^2 and circularity of 0.15-1.00 to measure density and roundness.

Statistical Analysis

Contrast to noise ratio (C/N) data for each micro-CT scan was imported to SPSS (IBM SPSS Statistics, version 25, Armonk, NY). Students t-tests were run to understand the effects of liquid medium (PBS or EtOH), staining (with or without PTA) and scan-type (absorption and propagation imaging) on C/N, and between the two scan-types for each preparation technique (Table 1 (a)-(d)). Data are mean ± standard deviation unless otherwise stated. Contrast to noise values were normally distributed, as assessed by Q-Q plot inspection. By inspection of boxplots, 14 of the 20 groups contained a limited number of outliers further than 1.5 box lengths. These constituted at most 1.8% of all values per group and thus were included. There was non-homogeneity of variances for groups ($p < 0.0005$) as assessed by Levene's test for equality of variances therefore the Welch's t-test was chosen, for which equal variances are not assumed. Paired-sample t-tests were run on the C/N values for the two pairs of repeat scans of samples prepared with PBS+PTA and EtoH+PTA. There were no outliers in the PBS+PTA groups and two significant outliers were found in the EtOH+PTA data (comprised of n = 220 data points) which were not excluded. Assessment by Q-Q plot inspection showed normally distributed differences in C/N scores for both conditions.

Results

PPC imaging following PTA staining in EtOH yields greatest chondrocyte visualisation

Our data show that the most efficient combination of imaging modality, sample preparation medium and staining to resolve cellular details in articular cartilage was to use propagation phase contrast (PPC) scanning of samples stained with PTA in EtOH (**Fig. 3**.D). Cellular features in cartilage were also

visualised in samples stained with PTA prepared in PBS as well as in unstained samples stored in EtOH. For both scan types, C/N for samples in ethanol were higher than PBS ($p < 0.0001$, **Fig. 3**.A), and higher for samples stained in PTA compared to unstained samples ($p < 0.0001$, **Fig. 3**.B). The C/N score for ethanol was higher than PBS for both unstained ($p = 0.001$) and stained samples ($p < 0.0001$, **Fig. 3**.C). Propagation scanning increased C/N for all sample preparation methods (Fig. **3**.D). There was no difference between the pairs of repeat scans in either the PBS+PTA or EtOH+PTA samples ($p = 0.852$ and $p = 0.112$ respectively, **Fig. 3**.E), showing scan repeatability. Simultaneous imaging of subchondral bone and cartilage did not impede image quality.

[Suggested placement for Figure 3]

Depth-dependent properties

Contrast to noise ratio values through the height of each sample are shown in **Fig. 4**. A control was included as a measure of contrast variation in the surrounding matrix which was similar in both scanning methods. For most of the sample preparation techniques contrast improved using the propagation phase scanning method (**Fig. 4**.B) compared to the absorption scans (**Fig. 4**.A) and remained improved through most of the sample height.

[Suggested placement for Figure 4]

Reconstructed z-slice images from the micro-CT scans for each sample preparation method (**Fig. 5**) infer the same results as the C/N values suggest: that propagation phase contrast shows more clearly defined features (**Fig. 5**.B). Features are most clearly visualised with staining in the ethanol group. Features reduce in size and intensity throughout the sample height.

[Suggested placement for Figure 5]

Histological Validation

In order to validate our findings from micro-CT analysis, we performed image registration between micro-CT and conventional cartilage histology images of the same sample (**Fig. 6** and supplementary video). Both techniques allowed observation and quantification of similar cellular features (**Fig. 6**.B, D, E) and cellular distribution **Fig. 6**.C). We attempted to correlate cellular area between the two imaging methods, but the area of an individual cell was too sensitive to greyscale thresholding for this to be accurately feasible. However, the density of cellular features observed with micro-CT was between the values for chondrocytes and their lacunae in the histological images (**Fig. 6**.C) and cellular roundness was similar (**Fig. 6**.D).

[Suggested placement for Figure 6]

Depth-dependent feature analysis (n = 12) was carried out between micro-CT and histology (**Fig. 7**). Density of cellular features reduced with distance from the subchondral bone for both methods (**Fig. 7**.A, B, C). Roundness remained similar for both micro-CT and histology throughout the sample height (**Fig. 7**.D).

[Suggested placement for Figure 7]

Discussion

We report for the utility of a standard laboratory micro-CT scanner to visualise and quantify features of the chondrocyte population within intact articular cartilage in 3D. Histological staining was used to confirm these cartilaginous features observed by micro-CT at the cellular level. Images between both methods were successfully registered, confirming the location and distribution of features. Measurements of cellular density measured with micro-CT yielded values within the range of chondrocytes and their lacunae measured with histological images. Morphology was compared with cellular roundness, for which both techniques yielded similar values. Repeatability of measured C/N values was confirmed for both PBS and EtOH-stained samples. Imaging was successful using propagation phase contrast imaging with the sample maintained within a liquid environment and is compatible with either PBS or EtOH as a medium, achieving the aims of the study. It is pertinent also that we find that simultaneous imaging of hard and soft tissues did not impede image quality. Propagation phase contrast increases the contrast of individual chondrocytes compared to using absorption contrast. This offers researchers the opportunity to image chondrocyte distributions in 3D without specialised synchrotron equipment, enabling investigations such as chondrocyte morphology across grades of cartilage damage, 3D strain mapping techniques such as digital volume correlation to evaluate mechanical properties *in situ*, and models for 3D finite element analysis *in silico* simulations.

This study represents a complimentary addition to the growing body of evidence supporting the non-destructive imaging of the constituents of articular cartilage. Previous studies have differed in focus on other aspects of the cartilage structure[14]; involved the use of highly specialist synchrotron facilities[25, 27, 39]; or drying and dehydration that may change the organisation and mechanical properties of the tissue[16]. We have compared and quantified the output scans of samples prepared

using different preparation techniques and scanning signals. As with previous studies it was found that heavy metal staining provided an improvement in signal attenuation[6, 14]. The use of PBS as the medium during sample preparation and subsequent staining is atypical in previous literature and provides a more physiological environment than EtOH or formalin fixation. The visualised features in this study are comparable to those achieved for similarly prepared samples in micro-CT and synchrotron facilities using a similar voxel size[14, 25], and additionally can image the adjacent subchondral bone. For sample (e) which was processed with EtOH and PTA staining we found the cellular density of chondrocyte features to reduce from 663 mm^{-2} to 511 mm^{-2} when approaching the cartilage surface. An earlier study using confocal microscopy and sectioning of bovine samples found cellular density to follow a similar trend with the lowest density furthest from the articular surface[40]. We note that there was a discrepancy in density between the chondrocytes and their lacunae. A potential cause of this was damage incurred by sectioning and associated processing, this is avoided with non-destructive visualisation techniques such as micro-CT. Micro-CT values for roundness were approximately 7% higher than with histology. This may be due to partial volume effect artefacts observed with micro-CT scanning[41].

Our study has several limitations. Host tissue was stored frozen at -25 °C and thawed for use. Successful histological staining of nuclei and cells post-scanning suggest that tissue disruption is not any more extensive than would be expected in samples prepared in this way. Previous studies have reported no difference in mechanical properties between fresh and frozen soft tissues[42] yet testing the method works with fresh tissue would be beneficial. Currently, this method has only been applied to a small number of juvenile bovine samples, and future studies are needed to increase the sample size and to confirm that the method works with human articular cartilage. Penetration issues were experienced by virtue of the low-energy X-rays being easily absorbed by the sample and surrounding container, and the method is limited by specimen size. It was found that the thickness

of the sample container had an effect on the signal reaching the detector. Wall thickness was kept below 1 mm to reduce weakening of the signal. Given that samples were scanned within liquid, using containers of large internal diameter decreased the detected signal due to increased liquid volume. The largest samples we have scanned with this technique were 6 mm in diameter. This provided sufficient resolving power at the perimeters and centre of the sample but suffered from inconsistent signal quality in the intermediate region. The scans presented in this study include ≈ 2 mm of the bovine cartilage height in the volume of interest. Ideally the whole cartilage thickness would have been included yet owing to the large thickness of bovine cartilage we sought to preserve resolution where possible. For the absorption scans a pixel size of 3.5 µm was used, compared to 2 µm for the phase contrast scans. Ideally this variable would have been removed but limitations with the scanner required a larger pixel size. Scanning parameters could not be kept consistent between scans owing to differences in sample density due to the different preparation techniques. Attempts were made to keep the overall scanning time similar for all samples but differences in exposure time and number of projections may still have affected comparison between the scans. Previous studies have shown that ionizing radiation can have a significant effect on a range of measured properties in articular cartilage samples[43, 44], including its mechanical properties[45]; bone is also negatively affected[46]. Low energy X-rays interact with these low-density materials and cause more damage than high energy beams causing particular problems for the low voltages used throughout this study[47]. Further to this, the heating effect on the sample has been shown to affect protein structures and illicit physical shrinkage[48]. These effects could be reduced by limiting the number of projections, and therefore scanning time. Moini *et al*., have reported colour changes in amino acids upon irradiation[47], and we observed that some of the samples stored in EtOH and stained with PTA had a temporary blue hue after scanning. Further work is necessary to determine whether these observations have negative implications for this mode of imaging. Currently the method has been validated in 2D against histological sections, further work is recommended for validation against established 3D techniques such as confocal imaging.

Herein, we report a novel and validated non-destructive technique to visualise chondrocyte features through a region of several millimetres in articular cartilage. This enables an objective quantification of chondrocyte distribution and morphology in three dimensions allowing greater insight for investigations into studies of cartilage development, degeneration and repair. One such application of our method, is as a means to provide a 3D pattern in the cartilage which, when combined with digital volume correlation, could determine 3D strain gradient measurements enabling potential treatment and repair of cartilage degeneration. Moreover, the method proposed here will allow evaluation of cartilage implanted with tissue engineered scaffolds designed to promote chondral repair, providing valuable insight into the induced regenerative process.

Acknowledgements

The authors wish to thank Maria Parkes for providing specimens, Farah Ahmed and Brett Clark for their assistance with the micro-CT imaging, Lorraine Lawrence for histological sectioning and staining and Kiron Athwal for assistance with the statistical analysis.

Author contributions

Conceived and designed the experiments: JNC, JRTJ, UH

Performed the experiments: JNC, AG, SAF

Analysis and interpretation of the data: JNC, SAF, BJ, AAP, SMR, JRTJ, UH

Drafting of the article: JNC, JRTJ, UH

Critical revision of the article for important intellectual content: JNC, AG, SAF, BJ, AAP, SMR, JRTJ, UH

Final approval of the article: JNC, AG, SAF, BJ, AAP, SMR, JRTJ, UH

Obtaining of funding: SMR, JRTJ, UH

JNC (j.clark14@imperial.ac.uk), JRTJ (j.jeffers@imperial.ac.uk) and UH (u.hansen@imperial.ac.uk) take responsibility for the integrity of the work as a whole, from inception to finished article.

Role of the funding source

The authors gratefully acknowledge the financial support of EPSRC funding (EP/N025059/1) and the first author holds the Imperial College Class of 1964 Scholarship. The authors (BJ and AAP) are also indebted to Versus Arthritis (grant no. 20581) for their support. Beyond financial support, the funding sources had no involvement in the preparation of this manuscript.

Competing interest statement

The authors report no conflicts of interest.

References

1. Reeves HA. On the structure of the matrix of human articular cartilage. Br Med J 1876;2:616.
2. Guilak F, Ratcliffe A, Mow VC. Chondrocyte deformation and local tissue strain in articular cartilage: A confocal microscopy study. J Orthop Res 1995;13:410-21.
3. Bay BK. Methods and applications of digital volume correlation. Journal of Strain Analysis for Engineering Design 2008;43:745-760.
4. Mizutani R, Takeuchi A, Uesugi K, Takekoshi S, Osamura RY, Suzuki Y. X-ray microtomographic imaging of three-dimensional structure of soft tissues. Tissue Eng Part C Methods 2008;14:359-63.

5. Mizutani R, Suzuki Y. X-ray microtomography in biology. Micron 2012;43:104-15.
6. Pauwels E, Van Loo D, Cornillie P, Brabant L, Van Hoorebeke L. An exploratory study of contrast agents for soft tissue visualization by means of high resolution x-ray computed tomography imaging. J Microsc 2013;250:21-31.
7. Nagarajan MB, Coan P, Huber MB, Diemoz PC, Wismuller A. Phase contrast imaging x-ray computed tomography: Quantitative characterization of human patellar cartilage matrix with topological and geometrical features. Proc SPIE Int Soc Opt Eng 2014;9038.
8. Metscher BD. Microct for comparative morphology: Simple staining methods allow high-contrast 3d imaging of diverse non-mineralized animal tissues. BMC Physiol 2009;9:11.
9. Palmer AW, Guldberg RE, Levenston ME. Analysis of cartilage matrix fixed charge density and three-dimensional morphology via contrast-enhanced microcomputed tomography. Proc Natl Acad Sci U S A 2006;103:19255-60.
10. Mashiatulla M, Moran MM, Chan D, Li J, Freedman JD, Snyder BD, et al. Murine articular cartilage morphology and compositional quantification with high resolution cationic contrast-enhanced ct. Journal of Orthopaedic Research 2017;35:2740-2748.
11. Bansal PN, Joshi NS, Entezari V, Malone BC, Stewart RC, Snyder BD, et al. Cationic contrast agents improve quantification of glycosaminoglycan (gag) content by contrast enhanced ct imaging of cartilage. J Orthop Res 2011;29:704-9.
12. Xie L, Lin AS, Guldberg RE, Levenston ME. Nondestructive assessment of sgag content and distribution in normal and degraded rat articular cartilage via epic-microct. Osteoarthritis Cartilage 2010;18:65-72.
13. Saukko AEA, Honkanen JTJ, Xu W, Vaananen SP, Jurvelin JS, Lehto VP, et al. Dual contrast ct method enables diagnostics of cartilage injuries and degeneration using a single ct image. Ann Biomed Eng 2017.
14. Nieminen HJ, Ylitalo T, Karhula S, Suuronen JP, Kauppinen S, Serimaa R, et al. Determining collagen distribution in articular cartilage using contrast-enhanced micro-computed tomography. Osteoarthritis Cartilage 2015;23:1613-21.
15. Nemetschek T, Riedl H, Jonak R. Topochemistry of the binding of phosphotungstic acid to collagen. J Mol Biol 1979;133:67-83.
16. Kestila I, Thevenot J, Finnila MA, Karhula SS, Hadjab I, Kauppinen S, et al. In vitro method for 3d morphometry of human articular cartilage chondrons based on micro-computed tomography. Osteoarthritis Cartilage 2018;26:1118-1126.
17. Bravin A. Exploiting the x-ray refraction contrast with an analyser: The state of the art. Journal of Physics D-Applied Physics 2003;36:A24-A29.
18. Betz O, Wegst U, Weide D, Heethoff M, Helfen L, Lee WK, et al. Imaging applications of synchrotron x-ray phase-contrast microtomography in biological morphology and biomaterials science. I. General aspects of the technique and its advantages in the analysis of millimetre-sized arthropod structure. J Microsc 2007;227:51-71.
19. Wu J, Takeda T, Lwin TT, Momose A, Sunaguchi N, Fukami T, et al. Imaging renal structures by x-ray phase-contrast microtomography. Kidney Int 2009;75:945-51.
20. Boone MN, De Witte Y, Dierick M, Almeida A, Van Hoorebeke L. Improved signal-to-noise ratio in laboratory-based phase contrast tomography. Microsc Microanal 2012;18:399-405.
21. Chapman D, Thomlinson W, Johnston RE, Washburn D, Pisano E, Gmur N, et al. Diffraction enhanced x-ray imaging. Physics in Medicine and Biology 1997;42:2015-2025.
22. David C, Nohammer B, Solak HH, Ziegler E. Differential x-ray phase contrast imaging using a shearing interferometer. Applied Physics Letters 2002;81:3287-3289.
23. Lee YS, Heo EA, Jun HY, Kang SH, Kim HS, Lee MS, et al. Articular cartilage imaging by the use of phase-contrast tomography in a collagen-induced arthritis mouse model. Acad Radiol 2010;17:244-50.

24. Ruan MZ, Dawson B, Jiang MM, Gannon F, Heggeness M, Lee BH. Quantitative imaging of murine osteoarthritic cartilage by phase-contrast micro-computed tomography. Arthritis Rheum 2013;65:388-96.
25. Schulz G, Götz C, Deyhle H, Müller-Gerbl M, Zanette I, Zdora M-C, et al. Hierarchical imaging of the human knee. 2016;9967:99670R.
26. Schulz G, Götz C, Müller-Gerbl M, Zanette I, Zdora MC, Khimchenko A, et al. Multimodal imaging of the human knee down to the cellular level. Journal of Physics: Conference Series 2017;849:012026.
27. Tesarova M, Mancini L, Simon A, Adameyko I, Kaucka M, Elewa A, et al. A quantitative analysis of 3d-cell distribution in regenerating muscle-skeletal system with synchrotron x-ray computed microtomography. Sci Rep 2018;8:14145.
28. Moeini M, Decker SG, Chin HC, Shafieyan Y, Rosenzweig DH, Quinn TM. Decreased solute adsorption onto cracked surfaces of mechanically injured articular cartilage: Towards the design of cartilage-specific functional contrast agents. Biochim Biophys Acta 2014;1840:605-14.
29. Davis GR, Elliott JC. Artefacts in x-ray microtomography of materials. Materials Science and Technology 2006;22:1011-1018.
30. Schindelin J, Arganda-Carreras I, Frise E, Kaynig V, Longair M, Pietzsch T, et al. Fiji: An open-source platform for biological-image analysis. Nat Methods 2012;9:676-82.
31. Nieminen HJ, Gahunia HK, Pritzker KPH, Ylitalo T, Rieppo L, Karhula SS, et al. 3d histopathological grading of osteochondral tissue using contrast-enhanced micro-computed tomography. Osteoarthritis Cartilage 2017;25:1680-1689.
32. Bancroft J, Stevens A, Theory and practice of histological techniques 4ed. 1996: Edinburgh Churchill Livingstone.
33. Culling CFA, Handbook of histopathological and histochemical techniques. 3 ed. 1974: Butterworth & Co. 72.
34. Puchtler H, Waldrop FS, Valentine LS. Polarization microscopic studies of connective tissue stained with picro-sirius red fba. Beitr Pathol 1973;150:174-87.
35. Schmitz N, Laverty S, Kraus VB, Aigner T. Basic methods in histopathology of joint tissues. Osteoarthritis Cartilage 2010;18 Suppl 3:S113-6.
36. Karhula SS, Finnila MA, Lammi MJ, Ylarinne JH, Kauppinen S, Rieppo L, et al. Effects of articular cartilage constituents on phosphotungstic acid enhanced micro-computed tomography. PLoS One 2017;12:e0171075.
37. Welvaert M, Rosseel Y. On the definition of signal-to-noise ratio and contrast-to-noise ratio for fmri data. PLoS One 2013;8:e77089.
38. Arganda-Carreras I, Kaynig V, Rueden C, Eliceiri KW, Schindelin J, Cardona A, et al. Trainable weka segmentation: A machine learning tool for microscopy pixel classification. Bioinformatics 2017;33:2424-2426.
39. Zehbe R, Schmitt VH, Kirkpatrick CJ, Brochhausen C. High resolution x-ray tomography - three-dimensional characterisation of cell-scaffold constructs for cartilage tissue engineering. Materials Science and Technology 2015;31:167-173.
40. Jadin KD, Wong BL, Bae WC, Li KW, Williamson AK, Schumacher BL, et al. Depth-varying density and organization of chondrocytes in immature and mature bovine articular cartilage assessed by 3d imaging and analysis. J Histochem Cytochem 2005;53:1109-19.
41. Palacio-Mancheno PE, Larriera AI, Doty SB, Cardoso L, Fritton SP. 3d assessment of cortical bone porosity and tissue mineral density using high-resolution microct: Effects of resolution and threshold method. J Bone Miner Res 2014;29:142-50.
42. Woo SL, Orlando CA, Camp JF, Akeson WH. Effects of postmortem storage by freezing on ligament tensile behavior. J Biomech 1986;19:399-404.
43. Cicek E. Effect of x-ray irradiation on articular cartilage mechanical properties. Acta Physica Polonica A 2016;129:200-202.

44. Willey JS, Long DL, Vanderman KS, Loeser RF. Ionizing radiation causes active degradation and reduces matrix synthesis in articular cartilage. International Journal of Radiation Biology 2013;89:268-277.
45. Lindburg CA, Willey JS, Dean D. Effects of low dose x-ray irradiation on porcine articular cartilage explants. J Orthop Res 2013;31:1780-5.
46. Barth HD, Zimmermann EA, Schaible E, Tang SY, Alliston T, Ritchie RO. Characterization of the effects of x-ray irradiation on the hierarchical structure and mechanical properties of human cortical bone. Biomaterials 2011;32:8892-904.
47. Moini M, Rollman CM, Bertrand L. Assessing the impact of synchrotron x-ray irradiation on proteinaceous specimens at macro and molecular levels. Anal Chem 2014;86:9417-22.
48. Wang B, Pan B, Lubineau G. In-situ systematic error correction for digital volume correlation using a reference sample. Experimental Mechanics 2018;58:427-436.

Figure legends

Fig. 1. *Sample preparation methodology for the four preparation methods using osteochondral plugs extracted from a similar position in the bovine condyles.*

Table 1. Micro-CT scan parameters. All scans took place at 40kV and 75µA. AC = Absorption contrast, PPC = Propagation phase contrast signal. SOD = Source-to-Object Distance, ODD = Object-to-Detector Distance. No x-ray filters were used. The supplementary table provides a further breakdown of parameters for each individual sample and includes sources for each sample.

Fig. 2. *Methodology to extract contrast to noise (C/N) values in the micro-CT scans of osteochondral plugs. A volume of interest within the cartilage region of the osteochondral plug (A.) was scanned, as shown by the black dashed cube (B.). To measure changes through the cartilage height, eleven layers equally spaced 100 layers apart (≈ 200 µm; C.) were taken from within the 1000-layer thick z-stack and on each of these layers ten features were analysed with the Surface Plot Tool in ImageJ (denoted by dashed lines; D.) to extract the grayscale intensity as a function of distance from the cell (E.), resulting in 110 plots per sample. Greyscale values were processed in MATLAB: the amplitude of the signal ("A") was divided by the standard deviation of the noise ("N") to give the C/N. Images shown are for sample (d.1) EtOH+PTA with PPC.*

Fig. 3. *Contrast to noise (C/N) data, as described in Figure 2, was statistically analysed with t-tests in SPSS and displayed are mean contrast to noise ratio for the three variables: scan type (absorption and propagation), medium (PBS and EtOH) and staining (none and PTA-staining) with their 95% CIs. (A.) Between mediums for the two scan protocols C/N was greater for EtOH than the PBS in both scanning methods (both $p < 0.0001$) with mean differences of 1.243 (95% CI 0.709 to 1.778) for*

*absorption contrast and 6.231 (95% CI 5.772 to 6.690) for propagation contrast. (B.) Between unstained and unstained samples for the two scan protocols. For absorption contrast, staining increased C/N by a mean value of 2.325 ($p < 0.0001$, 95% CI 1.824 to 2.837) and by 7.202 ($p < 0.0001$, 95% CI 6.786 to 7.618) for the propagation method. (C.) Between mediums with and without staining. Unstained, there was an increase in the C/N of 0.524 ($p = 0.001$, 95% CI 0.220 to 0.828) using ethanol rather than PBS and when using PTA staining there was an increase of 6.279 ($p < 0.0001$, 95% CI 5.83 to 6.730). (D.) Mean contrast to noise values for all scans divided by preparation technique. PPC increase C/N for all groups compared to AC: (a) PBS by 0.400 ($p < 0.038$, 95% CI (0.022 to 0.779), (b) PBS+PTA by 2.490 ($p < 0.0001$, 95% CI 2.093 to 2.885), (c) EtOH by 3.654 ($p < 0.0001$, 95% CI 2.782 to 4.527) and (d) by 8.224 ($p < 0.0001$, 95% CI 7.686 to 8.762). (E.) Two repeat propagation scans were taken of samples from the PTA-stained groups. No difference in mean C/N was found with either medium: PBS had a mean difference of 0.058 ($p = 0.852$, 95% CI -0.560 to 0.676), EtOH had a mean difference of 1.183 ($p = 0.112$, 95% CI 0.281 to 2.648).*P < 0.05, **P < 0.001, ***P < 0.0001.*

Fig. 4. *Mean contrast to noise ratio (C/N) values (with 95% CIs) through the height of osteochondral plugs prepared with various methods and micro-CT scanned using the two Absorption Contrast* (A.) *and Propagation Phase* (B.) *protocols. Chondrocyte grayscale intensity (n = 10) was plotted across 11 scan layers per sample as described in* ***Fig. 2****. The scans included a depth of approximately 2 mm of articular cartilage mid-way through its height. 100 micro-CT slices equates to approximately 200 µm. For comparison, data collected without cellular features is given as a control for signal variation in the surrounding matrix.*

Fig. 5. *Comparison of image quality through the height of samples under the different sample preparation techniques and micro-CT protocols. Layer 1 is in the cartilage above the subchondral bone, and layer 950 is distally located closer to the articular surface. For illustrative purposes brightness was normalised between sets of images, all analysis was carried out on unedited images.*

Fig. 6. *Micro-CT comparison with histology. (A.) Reconstructed micro-CT volume and light microscopy (LM) histological slices (Alcian Blue, Masson's Trichrome; Picro-Sirius Red and Safranin O) of sample (e): 70% EtOH and PTA staining. The scale of the micro-CT and histology images is comparable. (B.) A high magnification region of interest between the two techniques is shown with symbols denoting corresponding features. Equivalent 500 x 500 µm areas were analysed between both methods (each n = 36) and mean values (with 95% CIs) are shown for cellular density (C.) and cellular roundness (D.). Measurements for lacunae encompass the chondrocytes and other cellular features.*

Fig. 7. *Reconstructed micro-CT slice of 1.97 µm thickness of osteochondral plug sample (e): 70% EtOH and PTA staining (A.), with higher magnification volume renderings of different regions through the height of the cartilage: deep, middle and superior (B.). Renderings are of a volume of 135 x 135 x 80 µm produced with Fiji's Volume Viewer. Measures of density (C.), and roundness (D.) were calculated over 500 x 500 µm areas at the three locations for both micro-CT and histology (n = 12). Measurements for lacunae encompass the chondrocytes and other cellular features. Displayed values are mean and 95% CIs.*

Figure_1

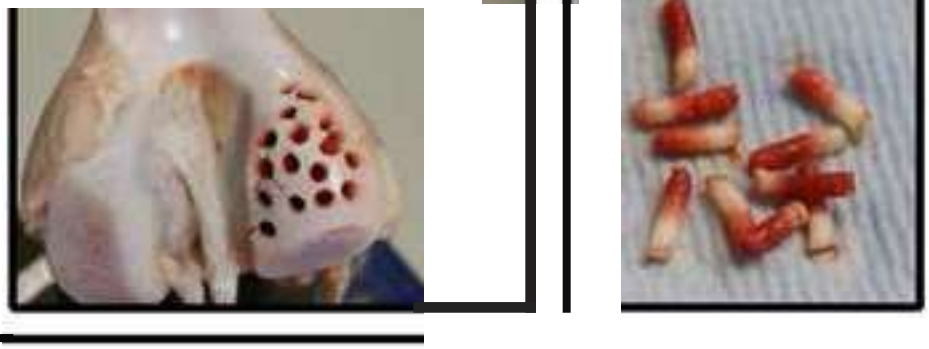

3mm diameter plugs from condyles

PBS 30 mins

25% EtOH 30 mins

50% EtOH 30 mins

...

70% EtOH 30 mins

...

1% PTA in PBS
21 hrs stain

1% PTA w/v
70% EtOH
21 hrs stain

Condition (a):
PBS

Condition (b):
PBS+PTA

Condition (c):
EtOH

Condition (d),(e):
EtOH+PTA

Micro-CT Scanning.Samples scanned in liquid

Histology (e)

Figure2

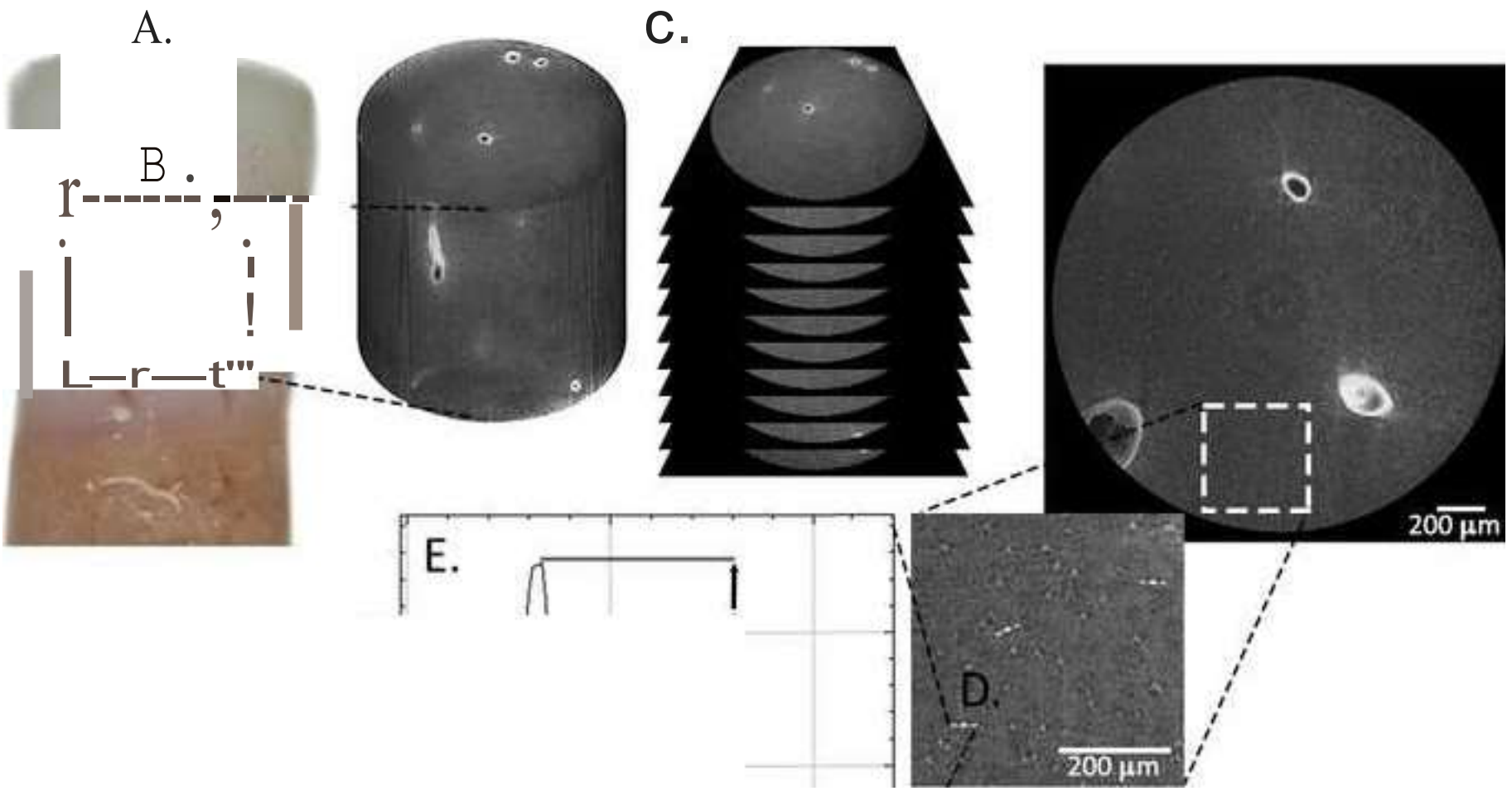

Figure3

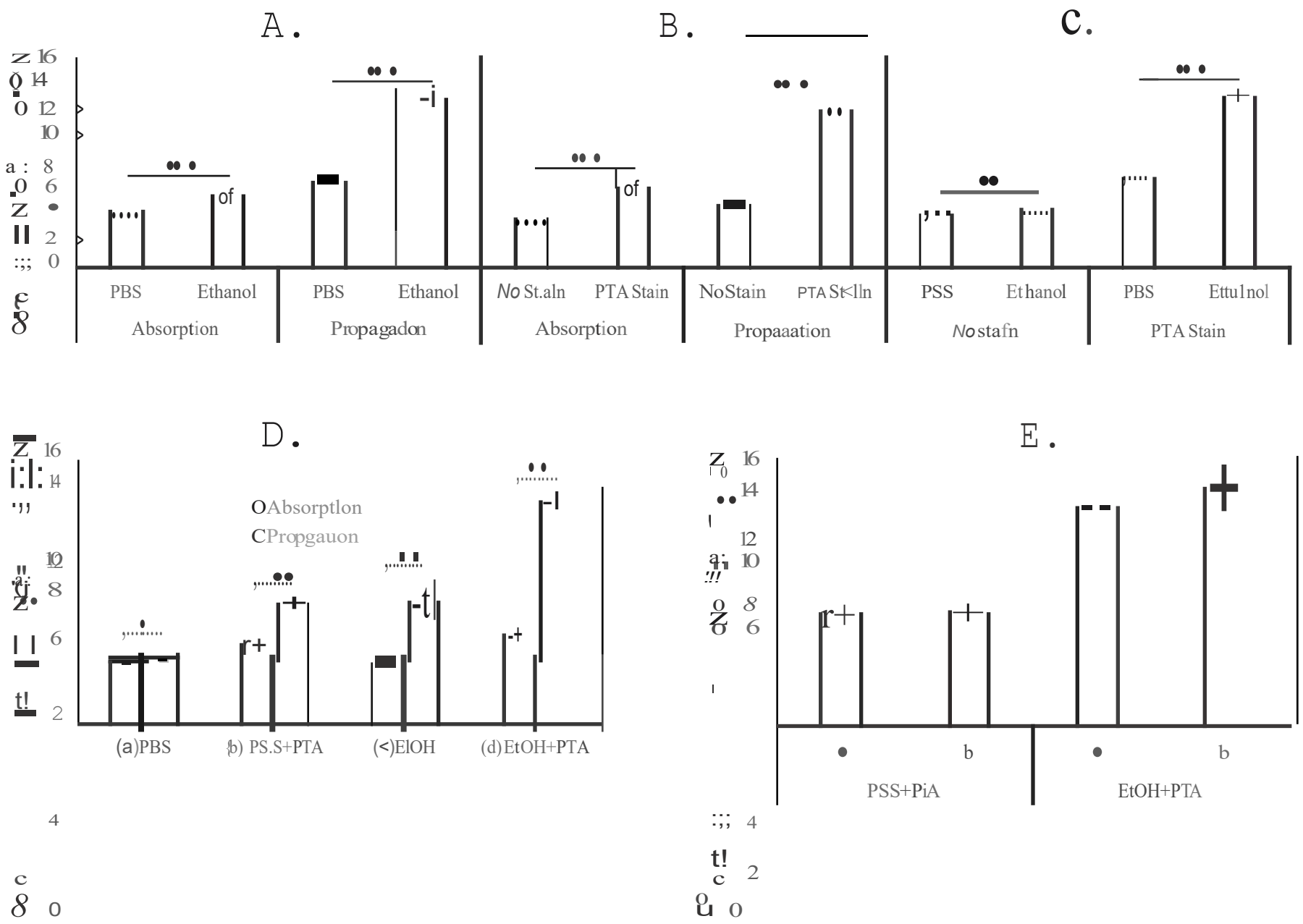
A.
B.
C.
PBS
Ethanol
Absorption
PBS
Ethanol
Propagadon
No St.aln
PTA Stain
Absorption
NoStain
PTA St<lln
Propaaation
PSS
Ethanol
Nostafn
PBS
Ettu1nol
PTA Stain
D.
OAbsorptlon
CPropgauon
(a)PBS
{b) PS.S+PTA
(<)ElOH
(d)EtOH+PTA
unstained
Ul\$tJined
E.
PSS+PiA
EtOH+PTA

Figure4

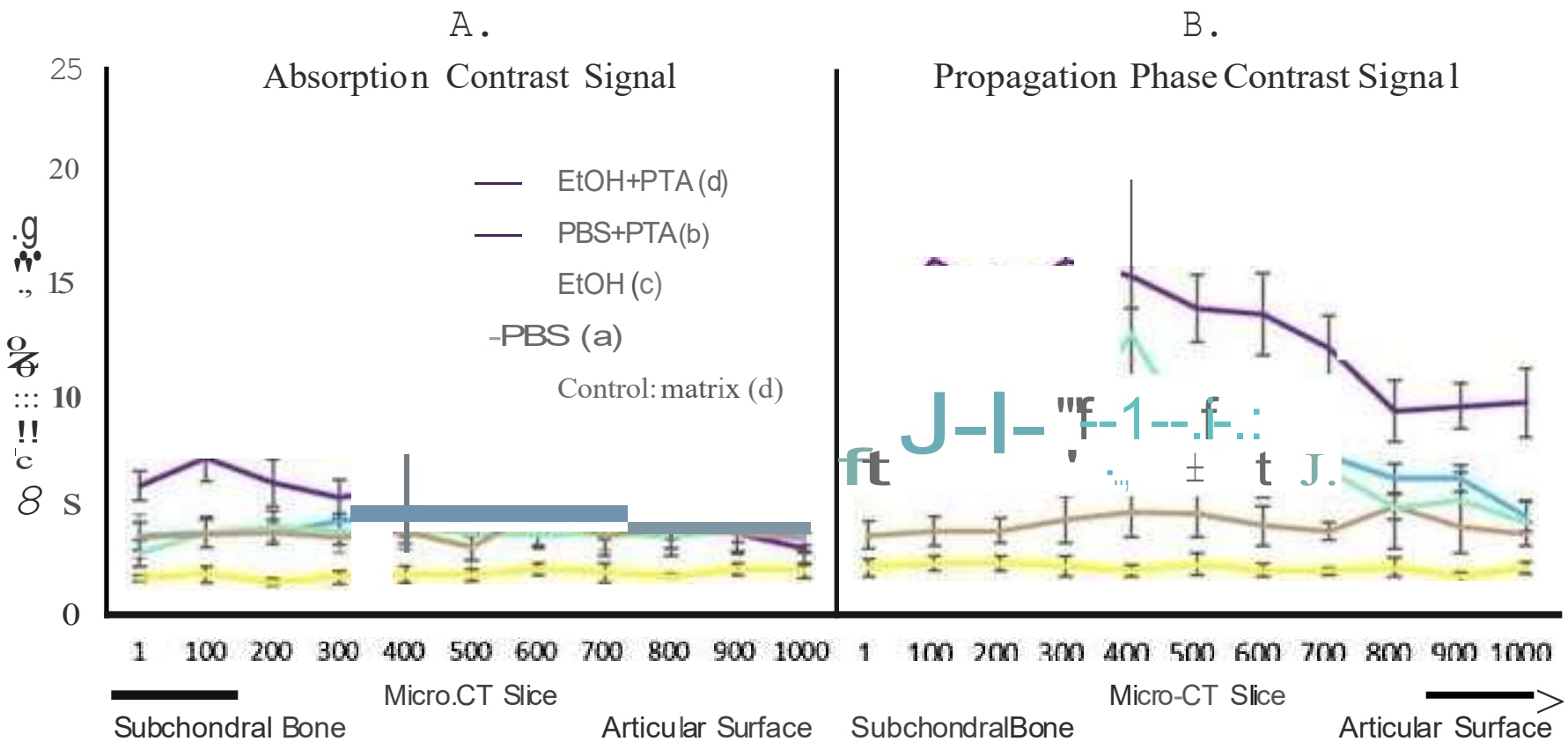
A.
Absorption Contrast Signal
B.
Propagation Phase Contrast Signal
25
20
15
10
0
EtOH+PTA (d)
PBS+PTA(b)
EtOH (c)
-PBS (a)
Control: matrix (d)
1 100 200 300 400 500 600 700 800 900 1000
1 100 200 300 400 500 600 700 800 900 1000
Micro.CT Slice
Micro-CT Slice
Subchondral Bone
Articular Surface
SubchondralBone
Articular Surface

Figure5

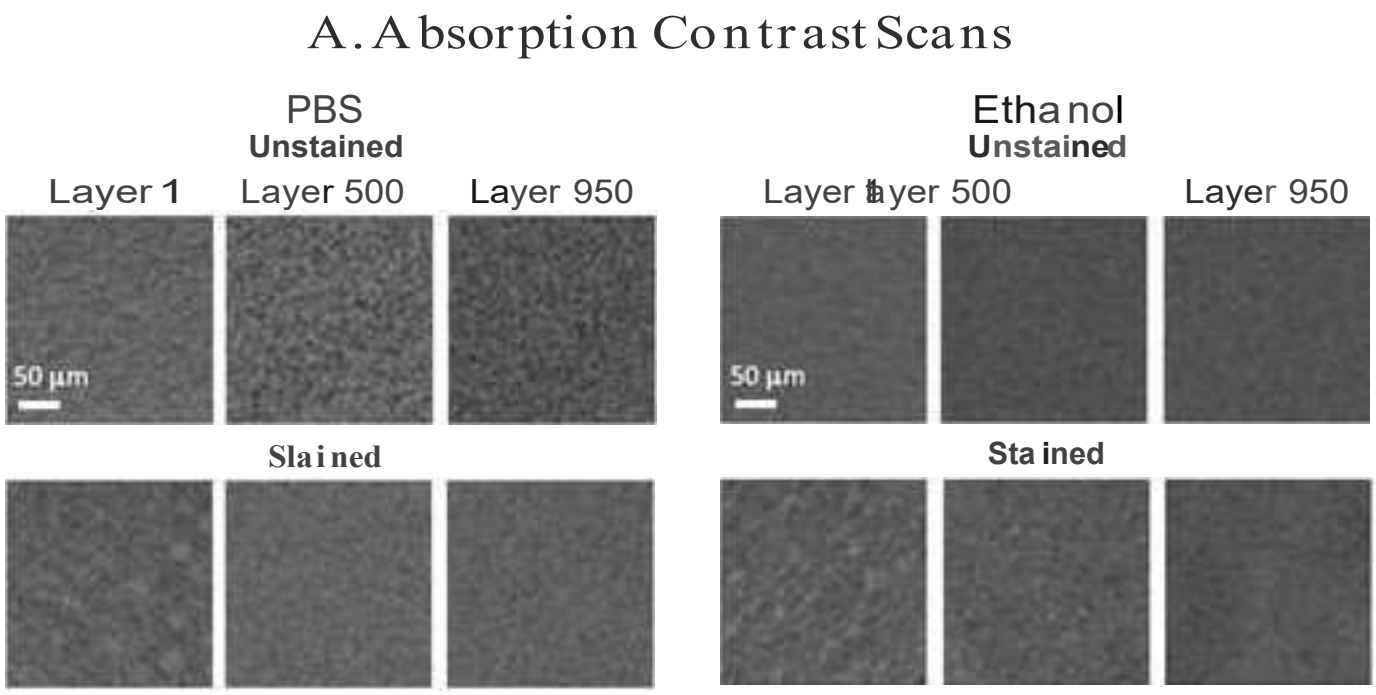
A. Absorption Contrast Scans
PBS
Unstained
Layer 1
Layer 500
Layer 950
50 µm
Stained
Ethanol
Unstained
Layer 1
Layer 500
Layer 950
50 µm
Stained
B. Propagation Phase Contrast Scans
PBS
Unstained
Layer 1
Layer 500
Layer 950
50 µm
Stained
Ethanol
Unstained
Layer 1
Layer 500
Layer 950
50 µm
Stained

Figure6

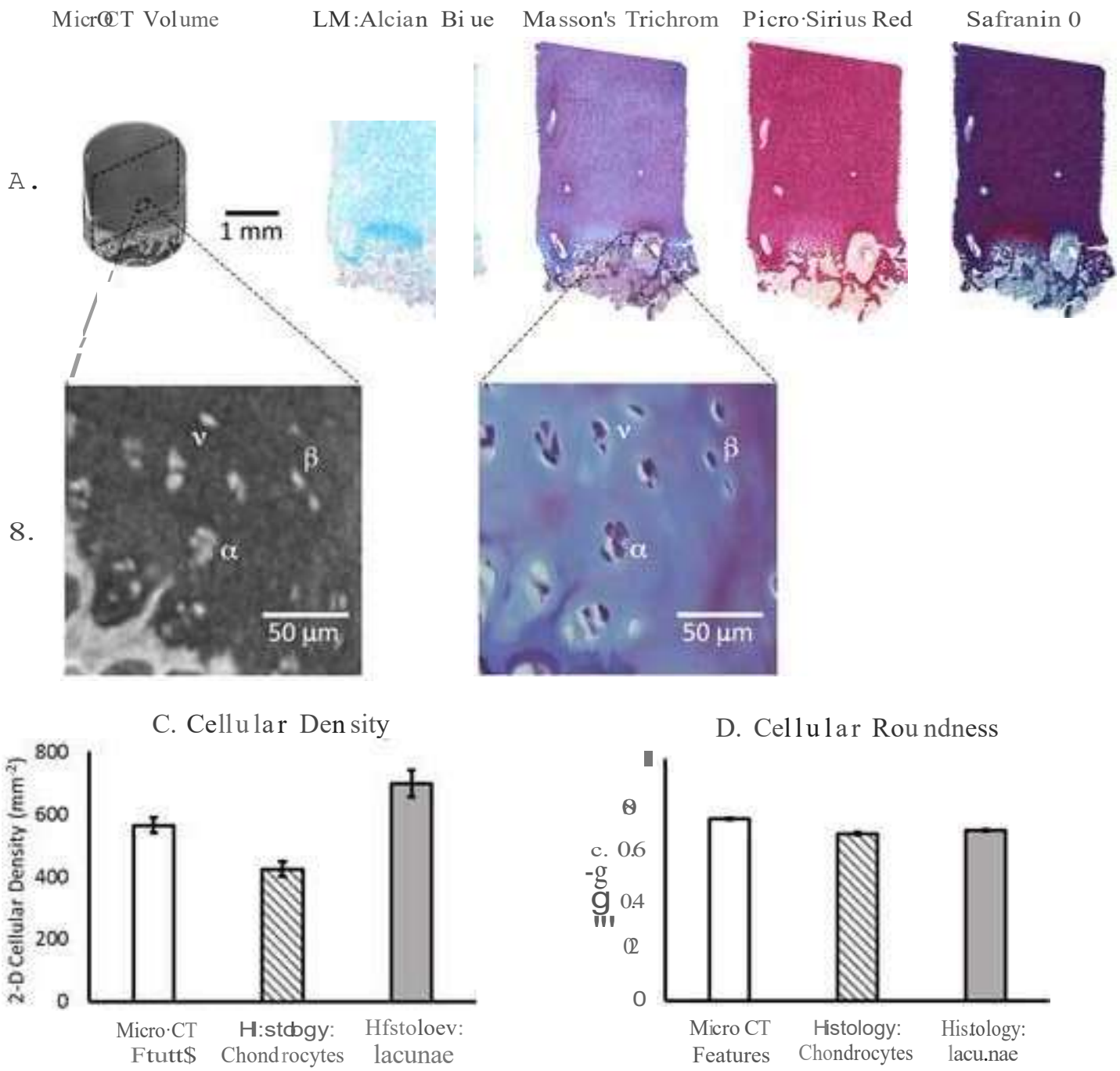
MicrCT Volume
LM:Alcian Bi ue
Masson's Trichrom
Picro·Sirius Red
Safranin 0
A.
1 mm
8.
ν
β
α
50 µm
ν
β
α
50 µm
C. Cellular Den sity
2-D Cellular Density (mm-2)
800
600
400
200
0
Micro·CT Ftutt$
H:stobgy: Chondrocytes
Hfstoloev: lacunae
D. Cellular Rou ndness
c. 0.6
0.4
0
Micro CT Features
Histology: Chondrocytes
Histology: lacu.nae

Figure7

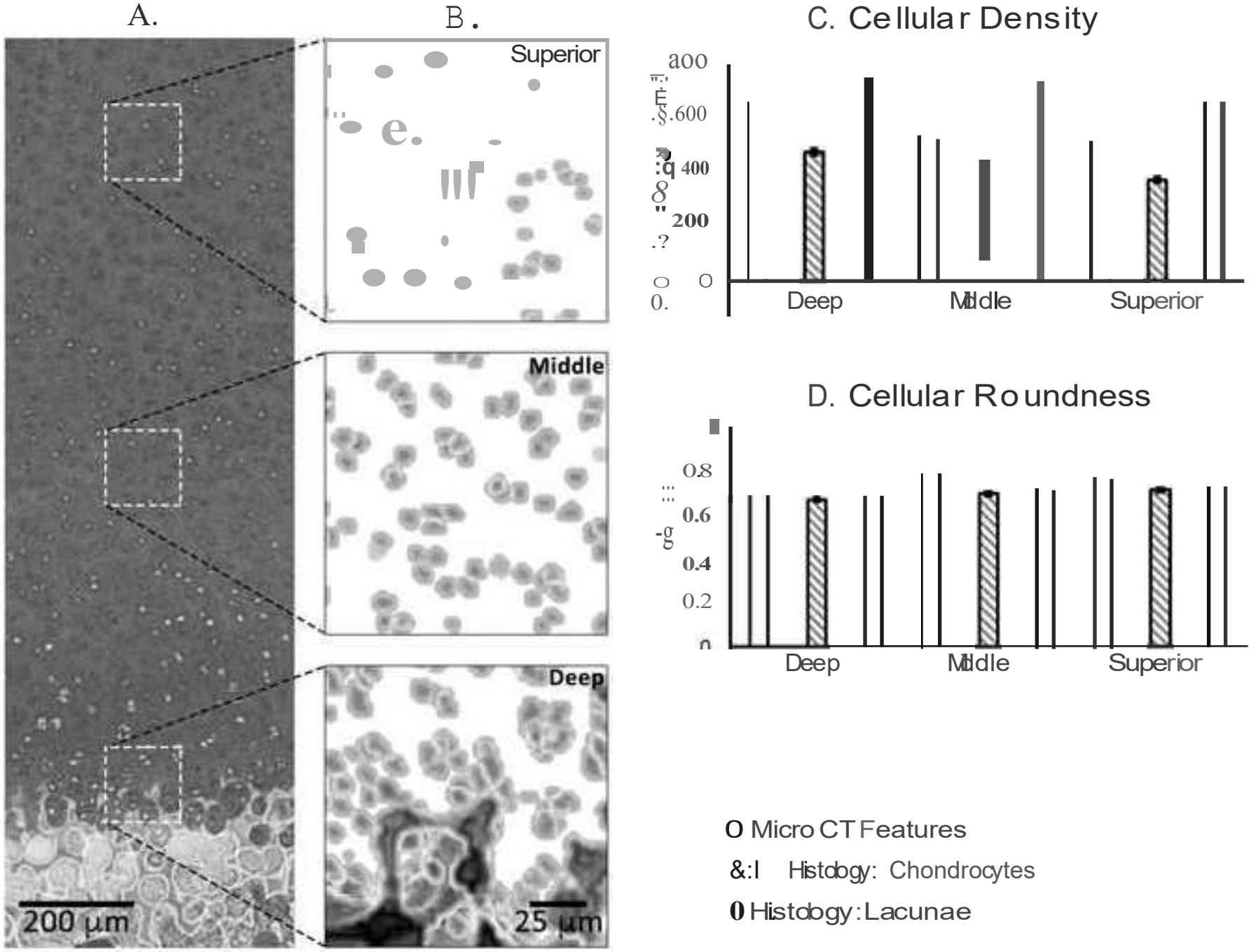
A.
B.
Superior
Middle
Deep
200 µm
25 µm
C. Cellular Density
Deep
Middle
Superior
D. Cellular Roundness
0.8
0.6
0.4
0.2
Deep
Middle
Superior
O Micro CT Features
Histology: Chondrocytes
Histology: Lacunae

Table 1. Micro-CT scan parameters. All scans took place at 40kV and 75µA. AC = Absorption contrast, PPC = Propagation phase contrast signal. SOD = Source-to-Object Distance, ODD = Object-to-Detector Distance. No x-ray filters were used. The supplementary table provides a further breakdown of parameters for each individual sample and includes sources for each sample.

Sample group	Method	Medium	Stain	n	Voxel (µm)	SOD (mm)	ODD (mm)	Exposure (s)	Projections
(a)	AC	PBS	-	1	3.53	20.0	18.0	5	2401
	PPC			1	1.99	23.5	55.8	22	2401
(b)	AC		PTA	1	3.53	20.0	18.0	8	2001
	PPC			3	1.97 - 2.09	23.5 - 25 .0	55.0 – 60.0	30 - 34	2001 - 3201
(c)	AC	EtOH	-	1	3.53	20.0	18.0	6	2301
	PPC			1	1.99	23.5	55.8	25	2301
(d)	AC		PTA	1	3.53	20.0	18.0	7	2001
	PPC			5	1.97 - 2.85	23.5 -30	40 - 73	25 - 40	2001 - 3201
(e)				1	1.97	30	73	30	3201

Table1 with changes marked

Table 1. Micro-CT scan parameters. All scans took place at 40kV and 75µA. AC = Absorption contrast, PPC = Propagation phase contrast signal. SOD = Source-to-Object Distance, ODD = Object-to-Detector Distance. No x-ray filters were used. The supplementary table provides a further breakdown of parameters for each individual sample and includes sources for each sample.

Sample group	Method	Medium	Stain	n	Voxel (µm)	SOD (mm)	ODD (mm)	Exposure (s)	Projections
(a)	AC	PBS	-	1	3.53	20.0	18.0	5	2401
	PPC			1	1.99	23.5	55.8	22	2401
(b)	AC		PTA	1	3.53	20.0	18.0	8	2001
	PPC			3	1.97 - 2.09	23.5 - 25 .0	55.0 – 60.0	30 - 34	2001 - 3201
(c)	AC	EtOH	-	1	3.53	20.0	18.0	6	2301
	PPC			1	1.99	23.5	55.8	25	2301
(d)	AC		PTA	1	3.53	20.0	18.0	7	2001
	PPC			5	1.97 - 2.85	23.5 -30	40 - 73	25 - 40	2001 - 3201
(e)				1	1.97	30	73	30	3201

Video Still